

Journal Pre-proof

High-entropy transition metal diborides by reactive and non-reactive spark plasma sintering: A comparative investigation

Giovanna Tallarita, Roberta Licheri, Sebastiano Garroni, Simone Barbarossa, Roberto Orrù, Giacomo Cao



PII: S0955-2219(19)30702-2

DOI: <https://doi.org/10.1016/j.jeurceramsoc.2019.10.031>

Reference: JECS 12793

To appear in: *Journal of the European Ceramic Society*

Received Date: 30 July 2019

Revised Date: 15 October 2019

Accepted Date: 16 October 2019

Please cite this article as: Tallarita G, Licheri R, Garroni S, Barbarossa S, Orrù R, Cao G, High-entropy transition metal diborides by reactive and non-reactive spark plasma sintering: A comparative investigation, *Journal of the European Ceramic Society* (2019), doi: <https://doi.org/10.1016/j.jeurceramsoc.2019.10.031>

This is a PDF file of an article that has undergone enhancements after acceptance, such as the addition of a cover page and metadata, and formatting for readability, but it is not yet the definitive version of record. This version will undergo additional copyediting, typesetting and review before it is published in its final form, but we are providing this version to give early visibility of the article. Please note that, during the production process, errors may be discovered which could affect the content, and all legal disclaimers that apply to the journal pertain.

© 2019 Published by Elsevier.

**High-Entropy Transition Metal Diborides by Reactive and Non-Reactive Spark Plasma Sintering:
a comparative investigation**

Giovanna Tallarita¹, Roberta Licheri¹, Sebastiano Garroni^{2,3}, Simone Barbarossa¹, Roberto Orrù^{1*}, and Giacomo Cao¹

*¹Dipartimento di Ingegneria Meccanica, Chimica, e dei Materiali, Unità di Ricerca del
Consorzio Interuniversitario Nazionale per la Scienza e Tecnologia dei Materiali
(INSTM), Università degli Studi di Cagliari, via Marengo 2, 09123 Cagliari, Italy*

*²Dipartimento di Chimica e Farmacia, Università degli Studi di Sassari, Via Vienna 2, 07100 Sassari,
Italy*

*³International Research Centre in Critical Raw Materials-ICCRAM, University of Burgos, Plaza Misael
Bañuelos s/n, 09001 Burgos, Spain*

*Corresponding author: Roberto Orrù - roberto.orrù@dimcm.unica.it

Abstract

The direct synthesis and consolidation by SPS (1950°C, 20min, 20MPa) of high-entropy $(\text{Hf}_{0.2}\text{Mo}_{0.2}\text{Zr}_{0.2}\text{Nb}_{0.2}\text{Ti}_{0.2})\text{B}_2$ from elemental powders resulted in a multiphase product. An increase of the heating rate determined a change of the mechanism governing the synthesis reaction from gradual solid-state diffusion to rapid combustion regime, while the final conversion degree was 67wt.%. The sintered product displayed a non-uniform microstructure with the presence of 10-15 μm sized pores, due to volatilization phenomena occurring during the combustion synthesis reaction. In contrast, when the SPS process was preceded by powder synthesis via SHS, a homogeneous single-phase ceramic was obtained. Clear benefits are derived by the use of SHS, able to provide very shortly powders with elemental species very well intermixed, so that the obtainment of $(\text{Hf}_{0.2}\text{Mo}_{0.2}\text{Zr}_{0.2}\text{Nb}_{0.2}\text{Ti}_{0.2})\text{B}_2$ during the subsequent SPS stage is strongly promoted. The resulting 92.5% dense product shows superior oxidation resistance with respect to individual borides prepared with the same method.

Keywords: High-entropy ceramics; Borides; Spark Plasma Sintering; Self-propagating High-temperature Synthesis; Resistance to oxidation.

1. Introduction

Due to their recent discovery and the huge potential they might provide in several emerging or traditional application areas, high-entropy (HE) ceramics have immediately gained a significant attention of the scientific community from both the experimental and theoretical points of view [1-27].

As for the general class of high-entropy alloys, HE ceramics are the result of the combination of different (at least four) individual constituents in near-equimolar percentages, where metal cations are incorporated into the lattice to generate single-phase crystalline solid solutions with maximum

configurational entropy [28,29]. The corresponding decrease of the Gibbs free energy makes the resulting material thermodynamically more stable at high temperatures. Besides the intrinsic interest for such novel ceramic's family, different studies have reported that members of HE materials exhibit superior hardness [4,5,9,10,16], elastic modulus [10] and oxidation resistance [4,23] properties as compared to the individual binary constituents.

The HE ceramic systems investigated so far include different oxides [1-3,7,8,12,17], carbides [5,6,10,12,16,23-27], borides [4,9,11,14,18,20-22], and silicides [15,19]. These studies are mostly devoted to the fabrication and characterization of these materials in bulk form, although few investigations are also specifically dedicated to the obtainment of HE ceramics as powders [13,18,27], or films [9]. In this context, Spark Plasma Sintering (SPS) has been largely considered for the preparation of massive bodies, due to the well know advantages associated to this technology [30,31].

The first study available in the literature on the synthesis of High-Entropy Borides (HEBs) was conducted by Gild and co-workers at the University of California, San Diego (USA) [4]. In the latter work, six different five-components HEBs were prepared via a double-stage process. The corresponding metal diborides (ZrB_2 , HfB_2 , TaB_2 , TiB_2 , MoB_2 , NbB_2 , and CrB_2) were first co-milled in equimolar proportions and the resulting powders consolidated for 5 min by SPS at 2000°C under an applied pressure of 30 MPa. The final samples displayed relative densities up to about 92.4%, with superior hardness and oxidation resistance properties with respect to the individual components processed under the same conditions. The contamination of some oxides was also reported to occur in most of the processed materials, for instance when considering $(Hf_{0.2}Mo_{0.2}Zr_{0.2}Nb_{0.2}Ti_{0.2})B_2$. More recently, the same group of authors proposed an alternative two-stage process for the preparation of $(Hf_{0.2}Zr_{0.2}Ta_{0.2}Nb_{0.2}Ti_{0.2})B_2$ [14]. The initial powders were first pre-sintered for 5 min at 1600°C and 30MPa and the resulting compact was processed by Flash-SPS with no die, using different electric power conditions (from 30 to 100% of the maximum level provided by their equipment). The addition of 3 wt.% graphite to the initial mixture was reported to reduce oxides content and improve product density

up to 99.3% of the theoretical level, being the latter one evaluated by assuming no loss of carbon during sintering. The obtained material consisted of the single hexagonal diboride phase along with small amounts of cubic carbide phase, formed due to graphite addition.

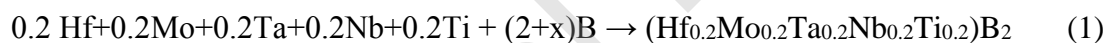
The fabrication of dense $(\text{Hf}_{0.2}\text{Zr}_{0.2}\text{Ta}_{0.2}\text{Cr}_{0.2}\text{Ti}_{0.2})\text{B}_2$, $(\text{Hf}_{0.2}\text{Mo}_{0.2}\text{Zr}_{0.2}\text{Nb}_{0.2}\text{Ti}_{0.2})\text{B}_2$, and $(\text{Hf}_{0.2}\text{Mo}_{0.2}\text{Ta}_{0.2}\text{Nb}_{0.2}\text{Ti}_{0.2})\text{B}_2$ was very recently accomplished by **Zhang et al. [21]**. Mixtures of transition metal oxides (HfO_2 , ZrO_2 , TaO_2 , etc.) and boron were first heat treated for 1h at 1600°C in vacuum, and the resulting product was processed in Argon by SPS for 10 min at 2000°C , and 30MPa. The resulting materials displayed relative densities above 95.5%, although the compositional homogeneity was not fully reached, particularly when considering the $(\text{Hf}_{0.2}\text{Mo}_{0.2}\text{Zr}_{0.2}\text{Nb}_{0.2}\text{Ti}_{0.2})\text{B}_2$, and $(\text{Hf}_{0.2}\text{Mo}_{0.2}\text{Ta}_{0.2}\text{Nb}_{0.2}\text{Ti}_{0.2})\text{B}_2$ systems. The fabrication of $(\text{Hf}_{0.2}\text{Zr}_{0.2}\text{Ta}_{0.2}\text{Nb}_{0.2}\text{Ti}_{0.2})\text{B}_2$, $(\text{Hf}_{0.2}\text{Zr}_{0.2}\text{Mo}_{0.2}\text{Nb}_{0.2}\text{Ti}_{0.2})\text{B}_2$, and $(\text{Hf}_{0.2}\text{Mo}_{0.2}\text{Ta}_{0.2}\text{Nb}_{0.2}\text{Ti}_{0.2})\text{B}_2$ was also investigated by the same authors using B_4C and C as reducing agents instead of B [22]. The materials obtained after SPS were reported to display relative densities of 96.3, 98.1 and 98.5%, respectively. Nonetheless, the weight fraction of the desired HEB phase was 94 % at most, while amounts of HfO_2 up to 7.0 wt.% were also found in the products. In addition, despite the XRD analysis results, the EDS maps clearly show that the agglomeration of certain species is often present across of the sintered samples [21,22]. Thus, the studies conducted so far evidenced that the fabrication of pure HEBs in massive form still represents a crucial issue.

In the present work, the reactive SPS (R-SPS) route is first considered for the synthesis and simultaneous consolidation of $(\text{Hf}_{0.2}\text{Mo}_{0.2}\text{Zr}_{0.2}\text{Nb}_{0.2}\text{Ti}_{0.2})\text{B}_2$ from elemental reactants. The effect produced by a change of the heating rates applied during the sintering process is also examined. As an alternative method, the same reaction promoters were first processed by Self-propagating High-temperature Synthesis (SHS) technique [32] for the preparation of the HE boride powders to be subsequently consolidated by SPS, thus considering the so-called SHS-SPS route. It should be noted that both the R-SPS and the SHS-SPS methods have been successfully employed in the last two decades by

our research group for the fabrication of various standard metal diborides in dense form, such as ReB₂ [33], TaB₂ [34,35], HfB₂ [36,37], ZrB₂ [35,38] and TiB₂ [39]. Very recently, preliminary results obtained when the SHS-SPS approach was attempted for the preparation of bulk (Hf_{0.2}Mo_{0.2}Zr_{0.2}Nb_{0.2}Ti_{0.2})B₂ were also reported in the literature [20]. In the present paper, the effect produced by various process parameters (dwell temperature, holding time, heating rate, mechanical load, etc.) on density, composition and microstructure of products obtained by R-SPS and SHS-SPS are addressed in detail. The oxidation resistance of the optimal massive HEB material is then compared with that one of individual diborides prepared following the same processing route and displaying similar relative density.

2. Materials and methods

The commercial powders used for R-SPS and SHS experiments are reported in **Table 1** along with the related characteristics provided by the suppliers. Mixing of reactants was performed according to the following reactions stoichiometry:



The use of an excess of B ($x > 0$) was also considered, based on previous outcomes found when synthesizing standard transition metal diborides following the same routes [25,35,38]. In addition, the effect produced by the reduction of Mo particles size was examined.

Powder mixing was carried out for 20 min in a SPEX 8000 (SPEX CertiPrep, USA) shaker mill using plastic vials and alumina balls. The obtained mixture was first cold-pressed to form cylindrical pellets, to be reacted inside a stainless-steel chamber filled with Argon, using an electrically heated tungsten filament as ignitor. Details of the SHS set-up and procedure can be found elsewhere [40]. The synthesis product was crashed in a mortar to convert it in powder form. The obtained powders were subsequently milled for different time intervals ($t_{BM} = 5-60$ min) using the milling device above, with

stainless steel vial and two steel balls (13 mm diameter, 8 g weight), being the resulting ball-to-powder weight ratio equal to 2. Particle size of the resulting powders was determined by laser light scattering analysis (CILAS 1180, France).

Reactive sintering experiments and the densification of SHS powders were both performed using a SPS apparatus (515S model, Fuji Electronic Industrial Co., Ltd., Kanagawa, Japan) under temperature-controlled mode and vacuum (20 Pa) conditions. About 4.4 g of powders were placed inside a hollow cylinder (30 mm external diameter; 15 mm inside diameter; 30 mm height) equipped with two punches (14.7 mm diameter, 20 mm height), all made of AT101 graphite (ATAL Srl., Italy). The temperature during SPS was measured by a C-type thermocouple (Fuji Electronic Industrial Co., Ltd., Kanagawa, Japan) inserted inside a small hole drilled on the lateral surface of the graphite die. An infrared pyrometer (CHINO, mod. IR-AHS2, Japan) focused on the lateral surface of the die was also used. The imposed thermal cycle consists of increasing the temperature from the room value to the maximum level (T_D) with a prescribed heating rate (HR), i.e. 100 or 200°C/min. The T_D value was then maintained constant for different dwell time periods (t_D) up to 20 min. The effect of T_D on the density and composition of the sintered product was investigated in the range 1800–1950 °C. The applied mechanical pressure was varied in the range 20–70 MPa. For the sake of reproducibility, each experiment was repeated at least twice.

Important information on the dynamics of the SPS process can be provided by the temporal changes of the recorded sample displacement. However, although the latter one is generally regarded as the degree of powder compact densification, thermal expansion of the sample, as well as that of both electrodes, graphite blocks, spacers and plungers, are also responsible for the variation of this parameter.

After SPS, the bulk samples were cut, ground and polished using progressively finer abrasive paper for further characterization. Their relative densities were evaluated by the Archimedes' method using distilled water as immersing medium and 8.67 g/cm³ as theoretical value [4].

Phases identification and structural characteristics of the synthesized powders and sintered products was carried by X-ray diffraction analysis (Philips PW 1830, Netherlands) using Cu K_{α} radiation, over a range of scattering angles 2θ from 20 to 130, in steps of 0.05° with 15 s acquisition time per angle. Phases content and the corresponding microstructural parameters were evaluated with the Rietveld method by analyzing the XRD patterns with the MAUD program [41].

The obtained SHS powders, R-SPS and SHS-SPS samples were also examined by high resolution scanning electron microscopy (HRSEM) (mod. S4000, Hitachi, Tokyo, Japan) equipped with a UltraDry EDS Detector (Thermo Fisher Scientific, Waltham, MA, USA).

The oxidation resistance of the $(\text{Hf}_{0.2}\text{Mo}_{0.2}\text{Ta}_{0.2}\text{Nb}_{0.2}\text{Ti}_{0.2})\text{B}_2$ product was evaluated by thermogravimetric analysis (NETZSCH, STA 409PC Luxx Simultaneous DTA-TGA Instrument, Germany) under 0.1 L/min air flow. Non-isothermal (dynamic) measurements, consisting of slowly heating ($2^{\circ}\text{C}/\text{min}$) the HEB sample from room temperature to 1450°C , as well as isothermal runs at 1200°C for about 4 h, have been carried out. For the sake of comparison, some individual diborides, namely HfB_2 , TaB_2 , and TiB_2 , prepared by SPS and characterized by similar relative densities, were also tested by DTA-TGA.

3. Results and discussion

3.1. Bulk HEBs via Reactive Spark Plasma Sintering

In principle, the most convenient and direct way to produce massive ceramic bodies is to perform material synthesis and densification in a single processing step. Accordingly, this approach was first attempted in this work for the preparation of bulk $(\text{Hf}_{0.2}\text{Mo}_{0.2}\text{Ta}_{0.2}\text{Nb}_{0.2}\text{Ti}_{0.2})\text{B}_2$. To this, elemental reactants mixed in stoichiometric ratio ($x=0$ in Eq. 1) were first processed by R-SPS under the conditions of $T_D = 1950^{\circ}\text{C}$, $t_D = 20$ min, $P=20$ MPa and $HR = 100^{\circ}\text{C}/\text{min}$. The temperature time profile imposed during the process is plotted in **Fig.1a** along with the related sample displacement. **Fig.1b**

shows the corresponding gas pressure evolution inside the SPS chamber during the process which provides important information, as discussed subsequently. Negative values in the displacement data are obtained at the initial stage of the R-SPS process. This outcome can be readily motivated by the thermal expansion contribution of the entire system (sample/die/plungers/spacers/electrodes) to the recorded displacement, which overcomes, during this period, that one (positive) due to powder densification. On the other hand, the displacement starts to increase after about 12 min from the beginning of the electric current application, when the temperature is approximately 1200°C. Afterward, this parameter is observed to raise in a gradual manner, first with a nearly constant rate and then with a decreasing one, until the end of the process. The absolute density of the final R-SPS product was $8.07 \pm 0.01 \text{ g/cm}^3$, corresponding to a relative density of about 93%.

The compositional changes of the powders undergoing R-SPS was monitored by XRD analysis. In particular, the corresponding patterns of the product obtained for $t_D = 20 \text{ min}$ is plotted in **Fig. 2** with that of the starting mixture. The $(\text{Hf}_{0.2}\text{Mo}_{0.2}\text{Ta}_{0.2}\text{Nb}_{0.2}\text{Ti}_{0.2})\text{B}_2$ content in the sintered material at the end of the process ($t_D = 20 \text{ min}$) was about 63.7% (**Table 2**), to indicate that reaction (1) does not go to completion. As also reported in **Table 2**, the weight percentage of the desired high-entropy boride phase in the product when $t_D = 5 \text{ min}$ ($t=t_1$ in **Fig. 1**) was approximately 54 wt.%, suggesting that the chemical transformation of initial reactants takes place gradually during the process. As shown in supplementary **Table S1**, where details of the different phases content as well as the related microstructural parameters are reported, various metal borides, along with small amount (about 2 wt.%) of HfO_2 , are also detected by XRD analysis.

The effect produced by an increase of the heating rate from 100 to 200°C/min is then examined. The SPS output shown in **Fig. 3a-3b** evidences that a different behavior is displayed by the reacting system with respect to the case when the dwell temperature is approached at a slower rate (**Fig. 1a**). Indeed, a sharp sample displacement takes place after approximately 3.2 min (t^*) during the non-isothermal stage conducted at 200 °C/min (**Fig. 3a**). This event is observed to occur when the measured temperature was

slightly above 600°C. The inset in **Fig. 3a** also evidenced that a slight local temperature increase, with respect to the scheduled thermal cycle, is correspondingly recorded. Moreover, after t^* the δ parameter decreases for a certain period. Furthermore, during such short time interval, the gas pressure inside the sintering chamber raised rapidly to relatively high levels (**Fig. 3b**), if compared to the case when the R-SPS process was performed at 100°C/min (**Fig. 1b**) where, albeit some changes of this parameter were observed in the course of the experiment, its value did not exceed 80 Pa. Based on all these features, it is apparent that a combustion synthesis-like reaction, accompanied by a local heat release with a subsequent sample expansion, took place at t^* . The latter statement is undoubtedly supported by the corresponding sudden compositional change, as evidenced by XRD analysis, whose results are shown in **Fig. 4**. In particular, as shown in **Table 2**, the Rietveld analysis indicated that the product correspondingly obtained for $x = 0$ is composed of 58.8% of $(\text{Hf}_{0.2}\text{Mo}_{0.2}\text{Ta}_{0.2}\text{Nb}_{0.2}\text{Ti}_{0.2})\text{B}_2$, with various secondary boride phases and HfO_2 (see supplementary **Table S1**). According to previous studies addressed in the literature to the preparation of standard diborides (ZrB_2 , HfB_2 , etc.) by R-SPS [35,36,38], where the use of a slight excess of boron (5-10 mol%) is usually beneficial to compensate the loss of this reactant due of the presence of some oxides and impurities in the raw powders, the x parameter in Eq. 1 was increased up to 0.2. Consistently, as shown in **Fig. 4**, the latter x value is found to improve the composition of the R-SPS product, being the yield in the desired HEB in the product at t^* equal to 64.5%. Very important is the fact that no oxides are detected in the product prepared using such excess of boron (see supplementary **Table S1**). It is also found that the progress of the R-SPS process up to $t_D = 20$ min determined only a slight improvement in product composition, with a $(\text{Hf}_{0.2}\text{Mo}_{0.2}\text{Ta}_{0.2}\text{Nb}_{0.2}\text{Ti}_{0.2})\text{B}_2$ content equal to 66.7 wt.%.

As far as powder densification is concerned, rather low densities (about 5.7 g/cm³) were reached at the end of the R-SPS process, if the applied pressure was maintained equal to 20 MPa during the entire process duration. On the other hand, the initial application of higher mechanical loads is not appropriate, for safety and other reasons, when strongly exothermic systems prone to react under the combustion

synthesis regime are processed [38]. Following the approach suggested in the literature for similarly-behaving systems [34,36,42], a two-stage mechanical load cycle, where the mechanical load is augmented nearly after the occurrence of the combustion synthesis reaction (t^*), is therefore considered. The effect of such change in the applied pressure is investigated in the range 20-70 MPa and the obtained results are shown in **Fig. 5**. As the mechanical pressure is augmented from 20 to 40 MPa, the average value of the density rises significantly, up to 7.6 g/cm^3 , while a further increase to 70 MPa determines a relatively lower effect. Approximately 8 g/cm^3 dense samples are correspondingly accomplished. It should be noted that the variation of the x parameter was found to produce a very modest effect on sample density.

Phases distribution and the microstructure of the sintered materials were also examined by SEM coupled with EDX analysis. The obtained results agree with the XRD analysis and density measurements. Indeed, as shown in **Fig. 6a**, despite the reasonably good consolidation level reached at the end of the R-SPS process conducted under low heating rates (100°C/min), the non-uniform elemental distribution shown by EDS maps provides a clear indication that a single-phase product is very far from being achieved. Apparently, a slightly improvement in the distribution of Hf, Mo and Ta elements can be observed across the sample prepared at higher heating rates (200°C/min), albeit zones with higher local concentrations of Nb and Ti can be clearly seen (cf. **Fig. 6b**). In addition, product microstructure is characterized by the presence of some large isolated pores $10\text{-}15 \mu\text{m}$ sized (indicated by the arrow in **Fig. 6b**), along with several smaller ones. Such pores can be likely ascribed to the gases suddenly liberated during the occurrence of the combustion synthesis event. Indeed, the volatilization of some impurities initially present in the powders and/or generated during synthesis reactions takes place inside a nearly closed container, so that the produced gases could hardly escape and remain entrapped within the bulk product. Another negative aspect worth to be mentioned when considering the preparation of HEBs by R-SPS is the observed sample weight loss, which was found to reach values even exceeding 10 wt.%, for the case of synthesis reactions evolving under the combustion regime. Both

these drawbacks above could be readily associated to the gases liberated in a very short time interval, which determine a marked pressure increase inside the die, as shown in **Fig. 3b**. Consequently, part of the powders undergoing R-SPS are forced out of the die.

Another parameter that could play a beneficial role for promoting reaction completion during the R-SPS process is represented by particles size of initial reactants. Based on the data provided by the vendors (Table 1), Ti and Mo powders are relatively coarser with respect to the other ones used in this work. In addition, while Ti is expected to melt under the adopted R-SPS condition, the use of finer Mo powder could provide more valuable indication in this regard. Accordingly, additional R-SPS experiments using $< 44 \mu\text{m}$ sized Mo powders, obtained after sieving the original commercial ones, were carried out. The cross-sectional SEM micrograph and the related EDX elemental maps of the corresponding sample produced by R-SPS ($HR = 100 \text{ }^\circ\text{C}/\text{min}$, $T_D = 1950\text{A}$, $t_D = 20 \text{ min}$, $P = 20 \text{ MPa}$) is reported in supplementary Fig. S1. It is clearly seen that, a slight improvement in term of elemental distribution is attained with respect to the sample achieved under the same conditions, except for the use of coarser Mo powders (Fig. 3a). However, the sintered product appears still rather porous and not homogeneous, so that powder consolidation and, above all, the completeness of the reaction to provide the desired dense high-entropy single phase material by R-SPS, is far from being reached.

3.2. Powder preparation by SHS

Once the mixture of reactants combined according to Eq. (1) was locally ignited, a self-sustaining combustion front was generated. This behavior was typically observed when the same approach was considered for the synthesis of individual transition metal diborides, like TaB_2 [34], HfB_2 [37], TiB_2 [39], and ZrB_2 [35], and is readily due to their strong exothermic character, i.e. $(-\Delta H_f^0) = 209.200$, 335.975 , 323.800 , and 322.586 , kJ/mol, respectively [43]. The reaction front associated to Eq. (1) was found to propagate very fast (about 2 sec in a 20 mm high pellet), with an average velocity of 4.75 ± 0.25

mm/s, whereas the measured combustion temperature was 2150 ± 100 °C. The transformation of the initial reactants to the expected HEB phase was verified by analyzing the SHS product by XRD. The obtained results are shown in **Fig. 7** for different x values and the corresponding percentage of the detected phases are listed in supplementary **Table S2** along with the corresponding microstructural parameters. From the yield in $(\text{Hf}_{0.2}\text{Mo}_{0.2}\text{Ta}_{0.2}\text{Nb}_{0.2}\text{Ti}_{0.2})\text{B}_2$ summarized in **Table 2**, it is seen that a significant improvement in term of material composition was achieved when operating with an excess of boron equivalent to $x=0.2$ in Eq. 1. Indeed, under the latter condition, about 96 wt.% of elemental reactants are converted to the desired phase, as revealed by the Rietveld analysis. Minor amounts of other secondary phases, namely $(\text{Ta}_{0.5}\text{Ti}_{0.5})\text{B}_2$, $(\text{Hf}_{0.5}\text{Ti}_{0.5})\text{B}_2$, HfB_2 , as well as traces of HfO_2 , are also detected in the end product.

The produced powders were also examined by SEM and EDX analysis. **Fig. 8** evidenced that a good mixing level between the different elements is reached inside each grain. Nonetheless, some regions with relatively higher/lower metals content can be seen, to confirm that a single-phase product was not attained at the end of the SHS process.

3.3. Consolidation by Spark Plasma Sintering of SHS powders

Three sets of powders were prepared after ball milling the SHS product for 5, 20 and 60 min, respectively. The resulting particle size characteristics, as measured by laser scattering analysis, are reported in **Table 3**. The relatively coarse particles attained after 5 min are markedly refined when the treatment was prolonged to 20 min. In contrast, only minor changes were observed when the milling period duration was extended to 1 h.

The temporal sample displacement changes plotted in **Fig. 9** for the case of $t_{BM} = 20$ min along with the corresponding temperature profile indicate that SHS powders exhibits a gradual consolidation behavior during SPS ($T_D = 1950^\circ\text{C}$, $P = 20$ MPa, $HR = 200^\circ\text{C}/\text{min}$, and $t_D = 20$ min). It is seen that only negligible changes of the δ parameter are recorded up to 7 min, when the corresponding measured

temperature was about 1200°C. The compact is observed to mostly densify during the non-isothermal stage, while, after the T_D value is reached, sample consolidation continues at a lower rate until the end of the process ($t_D = 20$ min). A similar qualitative behavior was shown by the differently milled powders.

The effect of the dwell temperature on the density of SPS specimens resulting from these three groups of powders can be deduced from **Fig. 10**. As expected, product densification is progressively enhanced as the sintering temperature was augmented. The effect of milling time is mainly observed at relatively lower T_D values, whereas it tends to vanish when operating at 1950°C, particularly when the milling treatment was prolonged from 20 to 60 min. This outcome is consistent with the similar particles size of these two groups of powders (**Table 3**). It should be mentioned the fact that all the experiments described so far were carried out under an applied pressure of 20 MPa. Nonetheless, as reported in supplementary **Fig. S1-S2**, an increase of the latter parameter up to 45 MPa did not provide valuable beneficial effects.

Apart from the densification issue, the other relevant aspect to consider is represented by the composition of the sintered material, since the SHS powders to be consolidated did not consist exclusively of the desired HEB phase. From the XRD analysis of the SPS product obtained 1950°C, whose results are reported in **Fig. 11** along with those ones corresponding to the starting SHS powders milled for 20 min, it is seen that the synthesis reaction went to completion during SPS. Indeed, as summarized in **Table 2** (details can be found in supplementary **Table S2**), a single-phase product is finally achieved with no evidence of the presence of secondary borides, oxides, etc., species.

Important features can be deduced when examining the SEM micrographs and related EDS maps reported in **Fig. 12** for different holding temperatures and milled powders. First, from **Fig. 12a** it is apparent that samples sintered at 1850°C are characterized by a marked residual porosity, other than a non-uniform elements distribution across the sample. While, in accordance with data reported in **Fig. 11**, an increase of the T_D value to 1900°C determines a marked improvement in term of product densification, the homogenization of the high-entropy phase is still not adequate (**Fig. 12b**). The

temperature needs to be further raised to 1950°C for achieving a satisfactory uniformity in composition across the SPS sample (**Fig. 12c**), in addition to a reduction of residual porosity. Finally, **Fig. 12d** evidences that the prolonged milling treatment from 20 to 60 min is accompanied by a further improvement of product microstructure. This is likely due to the reduction of the diffusion distances between the various phases during the mechanical treatment, so that the distribution of elemental species within the sample volume is facilitated during SPS and product homogenization enhanced.

3.4. Oxidation behavior of sintered samples

The oxidation behavior of the optimal HEB samples obtained in this work, i.e. about 92.5% dense and consisting exclusively of $(\text{Hf}_{0.2}\text{Mo}_{0.2}\text{Ta}_{0.2}\text{Nb}_{0.2}\text{Ti}_{0.2})\text{B}_2$, was examined by performing dynamic and isothermal TGA experiments in air flow. The corresponding curves, expressed as normalized weight gain, are compared in **Fig. 13a-13b**, respectively, with the results relative to standard individual diborides prepared according the SHS-SPS route and characterized by similar relative densities, namely HfB_2 (92.8%), TaB_2 (94.4%), and TiB_2 (93.1%). The dynamic tests conducted up to 1450°C clearly indicated that the system more sensitive to the oxidizing environment is TiB_2 , whose curve starts to raise at about 450°C and displayed the larger weight gain, with respect to the other diborides, during the entire temperature interval investigated (**Fig. 13a**). Also TaB_2 shows, although at a lower level compared to TiB_2 , scarce resistance to oxidation, since its mass progressively increases for temperature higher than 600°C. In contrast, both HfB_2 and HEB specimens exhibit only moderate weight changes for temperature lower than 1200-1300°C. On the other hand, the HE ceramic oxidized markedly for temperatures exceeding 1300°C, as proven by the corresponding sudden raise of the related curve.

Based on the latter outcome, the isothermal TGA tests were conducted at 1200°C. In addition, the TiB_2 sample was not considered for such experiments, due to the behavior manifested by this system during oxidation experiments carried out under dynamic conditions. The corresponding results reported in **Fig. 13b** are fully consistent with those ones obtained from non-isothermal tests. Indeed, while the

TaB₂ sample was subjected to a significant mass gain during the test, both HfB₂ and the high entropy ceramic exhibited low and thermally stable oxidation rate. In this regard, it should be noted that the latter two specimens are both characterized by relatively lower relative densities with respect to TaB₂ and TiB₂, so that they are, in principle, more exposed to oxygen diffusion.

On the basis of the results described above, it is possible to conclude that the oxidation up to 1200°C of the monophasic UHTC materials taken into account in the present work occurs according to the following hierarchical order: TiB₂ > TaB₂ > HfB₂ > (Hf_{0.2}Mo_{0.2}Ta_{0.2}Nb_{0.2}Ti_{0.2})B₂. These finding agrees with the oxidation test results conducted for the same systems by **Gild et al. [4]** using a tube furnace at different temperatures under flowing dry air. In particular, the high-temperature oxidation performances of the high-entropy, hafnium-, tantalum-, and titanium diborides investigated by **Gild et al. [4]** followed the order obtained, as indicated above, in the present work.

4. Concluding remarks

The identification of efficient processing routes for the fabrication of pure and dense high-entropy diborides certainly represents a crucial problem for the development of this novel class of ceramics. However, since the pioneering work by **Gild et al. [4]**, various difficulties were encountered for their synthesis and consolidation. Accordingly, the same authors recently pointed out that the originally proposed intense mechanical treatment of the individual diborides constituents before their processing by SPS is not convenient, to avoid significant product contamination and oxidation [14].

In the present work, the one-step synthesis and consolidation by reactive SPS of (Hf_{0.2}Mo_{0.2}Ta_{0.2}Nb_{0.2}Ti_{0.2})B₂ using elemental powders was first investigated. The sintering process was conducted for 20 min at 1950°C under different heating rate conditions. When the temperature was increased to the maximum level at 100°C/min, the transformation of reactants occurred through a gradual solid-state diffusion mechanism. In contrast, if heating rates equal to 200 °C/min are set, the synthesis reaction evolved under the combustion regime. In both cases, the synthesis reaction did not go

to completion, with a conversion of reactants to the desired high-entropy phase of about 67 wt.%, at most, although a good densification level was achieved, i.e. 91.3-93% relative density. SEM and EDS analysis confirmed that the obtainment of a single-phase product is far from being reached. In addition, isolated large pores were found in the sintered material when combustion synthesis reactions took place during the R-SPS process.

Significant improvement in the high-entropy material characteristics are obtained when the elemental powders were first reacted in few seconds by SHS and subsequently processed by SPS. As for the first step, the best result was reached when using 10 mol% excess of boron, with respect to the stoichiometric value, which allowed us to achieve about 96% conversion of initial reactants to $(\text{Hf}_{0.2}\text{Mo}_{0.2}\text{Ta}_{0.2}\text{Nb}_{0.2}\text{Ti}_{0.2})\text{B}_2$. Moreover, when the resulting powders were then processed by SPS for 20 min at 1950°C and 20 MPa, a 92.5% dense single-phase material was produced. The obtainment of a homogeneous material was clearly proven by accurate XRD analysis coupled with the Rietveld analytical procedure, SEM observations and EDS. Currently, work is on progress to further increase the densification level of the sintered product. In this regard, but also with the aim of promoting the completeness of the synthesis reaction during SHS and R-SPS processes, the use of finer reactants powder will be considered in further investigations. Nonetheless, the fact that no trace of secondary phases was found in the bulk material produced in this work represents a very important achievement, if compared with the results reported so far in the literature for the HEB taken into account. For instance, the oxides contamination was reported in the 92.2% dense $(\text{Hf}_{0.2}\text{Mo}_{0.2}\text{Ta}_{0.2}\text{Nb}_{0.2}\text{Ti}_{0.2})\text{B}_2$ material obtained by **Gild et al. [4]**. In addition, despite of the higher density level (98.5%) recently reached by **Zhang et al. [22]** for the same system, the yield in the high-entropy phase was 93 wt.% only, with about 7 wt.% hafnium oxides. The latter impurity was also detected by XRD analysis in the 95% dense material prepared by the same authors, using B, instead of B_4C and C, as precursors for the boro-thermal reduction of metal oxides [21]. Furthermore, EDX compositional maps evidenced that some species, mainly Nb, are not homogeneously distributed across the sample volume.

The results deriving from dynamic and isothermal oxidation tests carried out on the $(\text{Hf}_{0.2}\text{Mo}_{0.2}\text{Ta}_{0.2}\text{Nb}_{0.2}\text{Ti}_{0.2})\text{B}_2$ material obtained by SHS-SPS are rather promising, if compared to those ones relative to individual Ta-, Ti-, and Hf diborides produced with the same processing method and displaying slightly higher relative densities. In this regard, it is well recognized that metal borides are not able to withstand oxidative environments at high temperature, unless appropriate, generally Si-containing, additives are introduced in the matrix. Nonetheless, the high-entropy ceramic was shown to exhibit, similarly to HfB_2 , very low and stable oxidation rate up to 1200°C , whereas TiB_2 and TaB_2 gain markedly their weight at lower temperatures, i.e. about 450 and 650°C , respectively. This outcome is very promising in view of the possible utilization of this ceramic for high temperature applications in aggressive conditions. Further improvements on this property are certainly expected, if samples with higher relative densities are made available.

Declaration of interests: none

The authors declare that they have no known competing financial interests or personal relationships that could have appeared to influence the work reported in this paper.

The authors declare the following financial interests/personal relationships which may be considered as potential competing interests:

Acknowledgements

The present work has been carried out in the framework of the ARCHIMEDES project sponsored by Regione Autonoma della Sardegna (Italy) - Fondo di Sviluppo e Coesione (FSC) 2014-2020 (Cod. RAS: RASSR88309, Cod. CUP: F76C18000980002). One of the authors (G.T.) performed her activity in the framework of the International PhD in Innovation Sciences and Technologies at the University of

Cagliari, Italy. One of us (G.C.) acknowledges the results obtained in this manuscript as quite important for the “Ithermal” and “Generazione E” projects, sponsored by Sardegna Ricerche, Italy (Cod. CUP: F21I18000130006) and by the Italian Ministry of Education, University and Research, Italy (Cod. CUP: B96G18000560005), respectively. Thanks are due to Mr. Daniele Lai and Mr. Gianluca Marongiu (University of Cagliari) for their technical assistance.

Journal Pre-proof

References

- [1] C.M. Rost, E. Sachet, T. Borman, A. Moballegh, E.C. Dickey, D. Hou, J.L. Jones, S. Curtarolo, J.-P. Maria, Entropy-stabilized oxides, *Nat. Commun.* 6 (2015) art. no. 8485.
<https://doi.org/10.1038/ncomms9485>
- [2] D. Bérardan, S. Franger, A.K. Meena, N. Dragoë, Room temperature lithium superionic conductivity in high entropy oxides, *J. Mater. Chem. A* 4 (2016) 9536-9541.
<https://doi.org/10.1039/C6TA03249D>
- [3] D. Bérardan, S. Franger, D. Dragoë, A.K. Meena, N. Dragoë, Colossal dielectric constant in high entropy oxides, *Phys. Status Solidi RRL* 10 (2016) 328-333.
<https://doi.org/10.1002/pssr.201600043>.
- [4] J. Gild, Y. Zhang, T. Harrington, S. Jiang, T. Hu, M.C. Quinn, W.M. Mellor, N. Zhou, K. Vecchio, J. Luo, High-Entropy Metal Diborides: A New Class of High-Entropy Materials and a New Type of Ultrahigh Temperature Ceramics *Sci. Rep.* 6 (2016) art. no. 37946.
<https://doi.org/10.1038/srep37946>
- [5] M. Castle, T. Csanádi, S. Grasso, J. Dusza, M. Reece, Processing and Properties of High-Entropy Ultra-High Temperature Carbides, *Sci. Rep.* 8 (2018) art. no. 8609.
<https://doi.org/10.1038/s41598-018-26827-1>
- [6] J. Dusza, P. Švec, V. Girman, R. Sedlák, E.G. Castle, T. Csanádi, A. Kovalčíková, M.J. Reece, Microstructure of (Hf-Ta-Zr-Nb)₂C high-entropy carbide at micro and nano/atomic level, *J. Eur. Ceram. Soc.* 38 (2018) 4303–4307. <https://doi.org/10.1016/j.jeurceramsoc.2018.05.006>
- [7] J. Gild, M. Samiee, J.L. Braun, T. Harrington, H. Vega, P.E. Hopkins, K. Vecchio, J. Luo, High-entropy fluorite oxides, *J. Eur. Ceram. Soc.* 38 (2018) 3578-3584.
<https://doi.org/10.1016/j.jeurceramsoc.2018.04.010>.

- [8] S. Jiang, T. Hu, J. Gild, N. Zhou, J. Nie, M. Qin, T. Harrington, K. Vecchio, J. Luo, A new class of high-entropy perovskite oxides, *Scripta Mater.* 142 (2018) 116-120.
<https://doi.org/10.1016/j.scriptamat.2017.08.040>
- [9] P.H. Mayrhofer, A. Kirnbauer, P. Ertelthaler, C.M. Koller, High-entropy ceramic thin films; A case study on transition metal diborides. *Scripta Mater.* 149 (2018) 93-97.
<https://doi.org/10.1016/j.scriptamat.2018.02.008>
- [10] X. Yan, L. Constantin, Y. Lu, J.-F. Silvain, M. Nastasi, B. Cui, (Hf_{0.2}Zr_{0.2}Ta_{0.2}Nb_{0.2}Ti_{0.2})C high-entropy ceramics with low thermal conductivity, *J. Am. Ceram. Soc.* 101(10) (2018) 4486-4491.
<https://doi.org/10.1111/jace.15779>
- [11] Y.-P. Wang, G.-Y. Gan, W. Wang, Y. Yang, B.-Y. Tang, Ab Initio Prediction of Mechanical and Electronic Properties of Ultrahigh Temperature High-Entropy Ceramics, *Phys. Status Solidi B* (2018) art. no. 1800011. <https://doi.org/10.1002/pssb.201800011>
- [12] Chellali M. R., A. Sarkar, S.H. Nandam, S.S. Bhattacharya, B. Breitung, H. Hahn, L. Velasco, On the homogeneity of high entropy oxides: An investigation at the atomic scale, *Scripta Mater.* 166 (2019) 58-63. <https://doi.org/10.1016/j.scriptamat.2019.02.039>
- [13] L. Feng, W.G. Fahrenholtz, G.E. Hilmas, Y. Zhou, Synthesis of single-phase high-entropy carbide powders, *Scripta Mater.* 162 (2019) 90–93. <https://doi.org/10.1016/j.scriptamat.2018.10.049>
- [14] J. Gild, K. Kaufmann, K. Vecchio, J. Luo, Reactive flash spark plasma sintering of high-entropy ultrahigh temperature ceramics, *Scripta Mater.* 170 (2019) 106-110.
<https://doi.org/10.1016/j.scriptamat.2019.05.039>
- [15] J. Gild, J. Braun, K. Kaufmann, E. Marin, T. Harrington, P. Hopkins, K. Vecchio, J. Luo, A high-entropy silicide: (Mo_{0.2}Nb_{0.2}Ta_{0.2}Ti_{0.2}W_{0.2})Si₂, *J. Materiomics* (2019) in press
<https://doi.org/10.1016/j.jmat.2019.03.002>
- [16] T.J. Harrington, J. Gild, P. Sarker, C. Toher, C.M. Rost, O.F. Dippo, C. McElfresh, K. Kaufmann, E. Marin, L. Borowski, P.E. Hopkins, J. Luo, S. Curtarolo, D.W. Brenner, K.S. Vecchio, Phase

- stability and mechanical properties of novel high entropy transition metal carbides. *Acta Mater.* 166 (2019) 271-280. <https://doi.org/10.1016/j.actamat.2018.12.054>
- [17] W. Hong, F. Chen, Q. Shen, Y.-H. Han, W.G. Fahrenholtz, L. Zhang, Microstructural evolution and mechanical properties of (Mg,Co,Ni,Cu,Zn)O high-entropy ceramics, *J. Am. Ceram. Soc.* 102(4) (2019) 2228-2237. <https://doi.org/10.1111/jace.16075>
- [18] D. Liu, T. Wen, B. Ye, Y. Chu, Synthesis of superfine high-entropy metal diboride powders, *Scripta Mater.* 167(1) (2019) 110-114. <https://doi.org/10.1016/j.scriptamat.2019.03.038>
- [19] Y. Qin, J.-X. Liu, F. Li, X. Wei, H. Wu, G.-J. Zhang, A high entropy silicide by reactive spark plasma sintering, *J. Adv. Ceram.* 8(1) (2019) 148-152. <https://doi.org/10.1007/s40145-019-0319-3>
- [20] G. Tallarita, R. Licheri, S. Garroni, R. Orrù, G. Cao, Novel processing route for the fabrication of bulk high-entropy metal diborides, *Scripta Mater.* 158 (2019) 100-104. <https://doi.org/10.1016/j.scriptamat.2018.08.039>
- [21] Y. Zhang, W.-M., Guo, Z.-B. Jiang, Q.-Q. Zhu, S.-K. Sun, Y. You, K. Plucknett, H.-T. Lin, Dense high-entropy boride ceramics with ultra-high hardness, *Scripta Mater.* 164 (2019) 135-139. <https://doi.org/10.1016/j.scriptamat.2019.01.021>
- [22] Y. Zhang, Z.-B. Jiang, S.-K. Sun, W.-M. Guo, Q.-S. Chen, J.-X. Qiu, K. Plucknett, H.-T. Lin, Microstructure and mechanical properties of high-entropy borides derived from boro/carbothermal reduction, *J. Eur. Ceram. Soc.* 39(13) (2019) 3920-3924. <https://doi.org/10.1016/j.jeurceramsoc.2019.05.017>
- [23] J. Zhou, J. Zhang, F. Zhang, B. Niu, L. Lei, W. Wang, High-entropy carbide: A novel class of multicomponent ceramics, *Ceram. Int.* 44(17) (2018) 22014-22018. <https://doi.org/10.1016/j.ceramint.2018.08.100>
- [24] X.-F. Wei, J.-X. Liu, F. Li, Y. Qin, Y.-C. Liang, G.-J. Zhang, High entropy carbide ceramics from different starting materials, *J. Eur. Ceram. Soc.* (2019) in press, <https://doi.org/10.1016/j.jeurceramsoc.2019.04.006>

- [25] B. Ye , T. Wen, M.C. Nguyen, L. Hao, C.-Z. Wang, Y. Chu, First-principles study, fabrication and characterization of $(\text{Zr}_{0.25}\text{Nb}_{0.25}\text{Ti}_{0.25}\text{V}_{0.25})\text{C}$ high-entropy ceramics, *Acta Mater.* 170 (2019) 15-23.
<https://doi.org/10.1016/j.actamat.2019.03.021>
- [26] B. Ye, T. Wen , D. Liu, Y. Chu, Oxidation behavior of $(\text{Hf}_{0.2}\text{Zr}_{0.2}\text{Ta}_{0.2}\text{Nb}_{0.2}\text{Ti}_{0.2})\text{C}$ high-entropy ceramics at 1073-1473 K in air, *Corrosion Sci.* 153 (2019) 327–332.
<https://doi.org/10.1016/j.corsci.2019.04.001>
- [27] B. Ye, S. Ning, D. Liu, T. Wen, Y. Chu, One-step synthesis of coral-like high-entropy metal carbide powders, *J. AM. Ceram. Soc.* (2019) in press <https://doi.org/10.1111/jace.16514>
- [28] M.-H. Tsai, J.-W. Yeh, High-entropy alloys: a critical review, *Mater. Res. Lett.* 2 (2014) 107-123.
<https://doi.org/10.1080/21663831.2014.912690>
- [29] Y.F. Ye, Q. Wang, J. Lu, C.T. Liu, Y. Yang, High-entropy alloy: challenges and prospects *Mater. Today*, 19 (2016) 349-362. <https://doi.org/10.1016/j.mattod.2015.11.026>
- [30] R. Orrù, R. Licheri, A.M. Locci, A. Cincotti, G. Cao, Consolidation/synthesis of materials by electric current activated/assisted sintering, *Mater. Sci. Eng. R* 63 (2009) 127-287.
<https://doi.org/10.1016/j.mser.2008.09.003>
- [31] Spark Plasma Sintering: Current Status, New Developments and Challenges. G. Cao, C. Estournés, J. Garay, R.Orrù Eds., published by Elsevier, ISBN: 978-0-12-817744-0 (2019)
<https://doi.org/10.1016/C2018-0-02428-7>
- [32] A. Varma, A.S. Rogachev, A. S. Mukasyan, A. S., S. Hwang, Combustion Synthesis of Advanced Materials: Principles and Applications, *Adv. Chem. Eng.* 24 (1998) 79-226.
[https://doi.org/10.1016/S0065-2377\(08\)60093-9](https://doi.org/10.1016/S0065-2377(08)60093-9)
- [33] A.M. Locci, R. Licheri, R. Orrù, G. Cao, Reactive Spark Plasma Sintering of Rhenium Diboride, *Ceram. Int.* 35(1) (2009) 397-400. <https://doi.org/10.1016/j.ceramint.2007.11.012>

- [34] C. Musa, R. Orrù, R. Licheri, G. Cao, Spark Plasma Synthesis and Densification of TaB₂ by Pulsed Electric Current Sintering, *Mater. Lett.* 65 (2011) 3080–3082.
<https://doi.org/10.1016/j.matlet.2011.06.094>
- [35] R. Licheri, C. Musa, R. Orrù, G. Cao, D. Sciti, L. Silvestroni, Bulk Monolithic Zirconium and Tantalum Diborides by Reactive and Non-reactive Spark Plasma Sintering, *J. Alloys Compd* 663 (2016) 351-359. <https://doi.org/10.1016/j.jallcom.2015.12.096>
- [36] C. Musa, R. Orrù, D. Sciti, L. Silvestroni, G. Cao, Synthesis, consolidation and characterization of monolithic and SiC whiskers reinforced HfB₂ ceramics, *J. Eur. Ceram. Soc.* 33 (2013) 603-614.
<https://doi.org/10.1016/j.jeurceramsoc.2012.10.004>
- [37] C. Musa, R. Licheri, R. Orrù, G. Cao, Synthesis, Sintering, and Oxidative Behavior of HfB₂-HfSi₂ Ceramics *Ind. Eng. Chem. Res.* 53(22) (2014) 9101-9108. <https://doi.org/10.1021/ie4032692>
- [38] R. Licheri, C. Musa, R. Orrù, G. Cao, Influence of the heating rate on the in-situ synthesis and consolidation of ZrB₂ by Reactive Spark Plasma Sintering, *J. Eur. Ceram. Soc.* 35(4) (2015) 1129–1137. <https://doi.org/10.1016/j.jeurceramsoc.2014.10.039>
- [39] E. Sani, M. Meucci, L. Mercatelli, A. Balbo, C. Musa, R. Licheri, R. Orrù, G. Cao, Titanium diboride ceramics for solar thermal absorbers, *Sol. Energy Mater Sol. Cells* 169 (2017) 313-319.
<https://doi.org/10.1016/j.solmat.2017.05.038>
- [40] A. Cincotti, R. Licheri, A.M. Locci, R. Orrù, G. Cao, A review on combustion synthesis of novel materials: recent experimental and modeling results, *J. Chem. Technol. Biotechnol.* 78 (2003) 122-127. <https://doi.org/10.1002/jctb.757>.
- [41] L. Lutterotti, R. Ceccato, R. Dal Maschio, E. Pagani, Quantitative analysis of silicate glass in ceramic materials by the Rietveld method, *Mater. Sci. Forum* 87 (1998) 278-281.
<https://doi.org/10.4028/www.scientific.net/MSF.278-281.87>
- [42] U. Anselmi-Tamburini, Y. Kodera, M. Gasch, C. Unuvar, Z.A. Munir, M. Ohyanagi, M. Johnson, Synthesis and characterization of dense ultra-high temperature thermal protection materials

produced by field activation through spark plasma sintering (SPS): I. Hafnium diboride, J Mater

Sci 41(10) (2006) 3097–3104. <https://doi.org/10.1007/s10853-005-2457-y>

[43] Barin I., Thermochemical data of pure substances. VHC, Weinheim, Germany, 1989.

Journal Pre-proof

Table 1. Characteristics of powder reactants used for reactive SPS and SHS experiments

Reactant	Vendor, code	Particle size (μm)	Purity (%)
Hf	Alfa Aesar, cod. 10201	< 44	99.6
Mo	Aldrich, cod 26.689-2	< 149	≥ 99
Ta	Alfa Aesar, cod 00337	< 44	99.9
Nb	Alfa Aesar, cod 010275	< 44	99.8
Ti	Aldrich, cod 26.849-6	< 149	99.7
B, amorphous	Aldrich, cod 15580	-	≥ 99

Table 2. HEB yields and related experimental conditions adopted in this work for the fabrication of $(\text{Hf}_{0.2}\text{Mo}_{0.2}\text{Ta}_{0.2}\text{Nb}_{0.2}\text{Ti}_{0.2})\text{B}_2$. Details of the secondary phases content and microstructural parameters are reported in supplementary **Table S1 and S2**.

Method	Sample type	B/Me ratio (<i>x</i>)	SPS conditions (<i>HR</i> , <i>T_D</i> , <i>t[*]/t_D</i> , <i>P</i>)	Yield in HEB (wt.%)
R-SPS	Bulk	0	100°C/min, 1950°C, <i>t_D</i> = 5 min, 20 MPa	54.1
R-SPS	Bulk	0	100°C/min, 1950°C, <i>t_D</i> = 20 min, 20 MPa	63.7
R-SPS	Powder	0	200°C/min, 1950°C, <i>t[*]</i> , 20 MPa	58.8
R-SPS	Powder	0.2	200°C/min, 1950°C, <i>t[*]</i> , 20 MPa	64.5
R-SPS	Bulk	0.2	200°C/min, 1950°C, <i>t_D</i> = 20 min, 20-70 MPa	66.6
SHS	Powder	0	-	36.7
SHS	Powder	0.1	-	47.1
SHS	Powder	0.2	-	96.2
SHS-SPS	Bulk	0.2	200°C/min, 1950°C, <i>t_D</i> = 20 min, 20 MPa	100

Table 3. Particle size characteristics, as determined by laser scattering analysis, of differently ball-milled HEB powders prepared by SHS.

<i>t_{BM}</i> (min)	<i>d</i> ₁₀ (μm)	<i>d</i> ₅₀ (μm)	<i>d</i> ₉₀ (μm)	<i>d</i> _{average} (μm)
5	0.53±0.12	7.41±1.43	35.69±5.21	13.31±1.90
20	0.22±0.03	1.94±0.14	9.83±0.38	3.72±0.19
60	0.20±0.04	1.49±0.13	8.76±0.53	3.16±0.26

Fig. 1 Temperature and sample displacement (a) time profiles and gas pressure (b) during reactive SPS of $(\text{Hf}_{0.2}\text{Mo}_{0.2}\text{Ta}_{0.2}\text{Nb}_{0.2}\text{Ti}_{0.2})\text{B}_2$ ($T_D = 1950\text{A}$, $P = 20\text{ MPa}$, $HR = 100^\circ\text{C}/\text{min}$, $t_D = 20\text{ min}$).

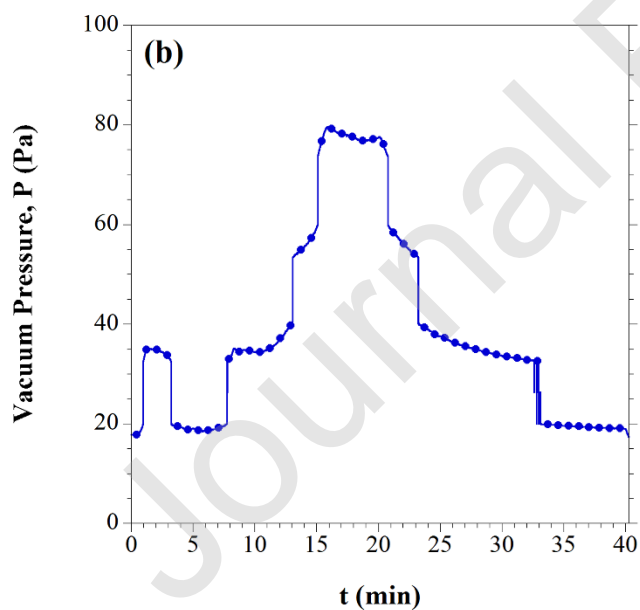
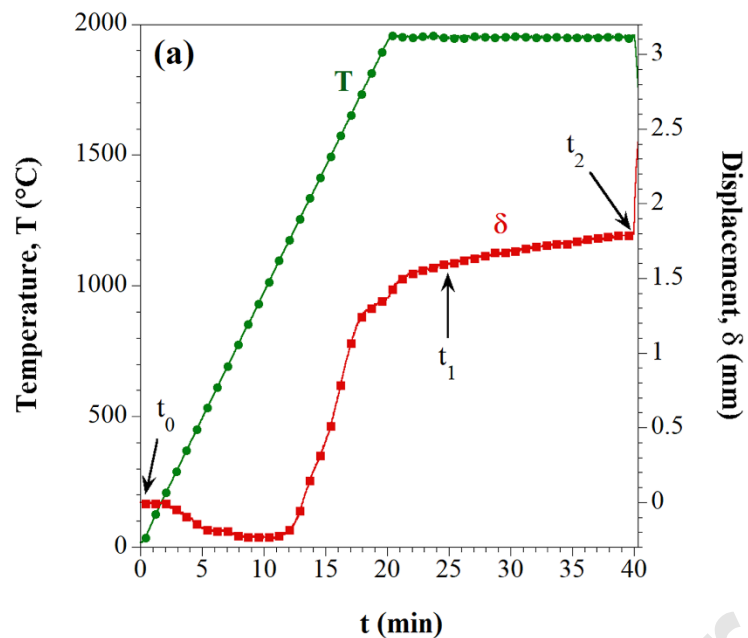


Fig. 2 XRD patterns of (a) reactants and (b) related SPS products ($T_D = 1950$ A, $P = 20$ MPa, $HR = 100^\circ\text{C}/\text{min}$, $t_D = 20$ min) obtained during reactive sintering of $(\text{Hf}_{0.2}\text{Mo}_{0.2}\text{Ta}_{0.2}\text{Nb}_{0.2}\text{Ti}_{0.2})\text{B}_2$, and corresponding to t_0 , and t_2 in **Fig. 1**, respectively.

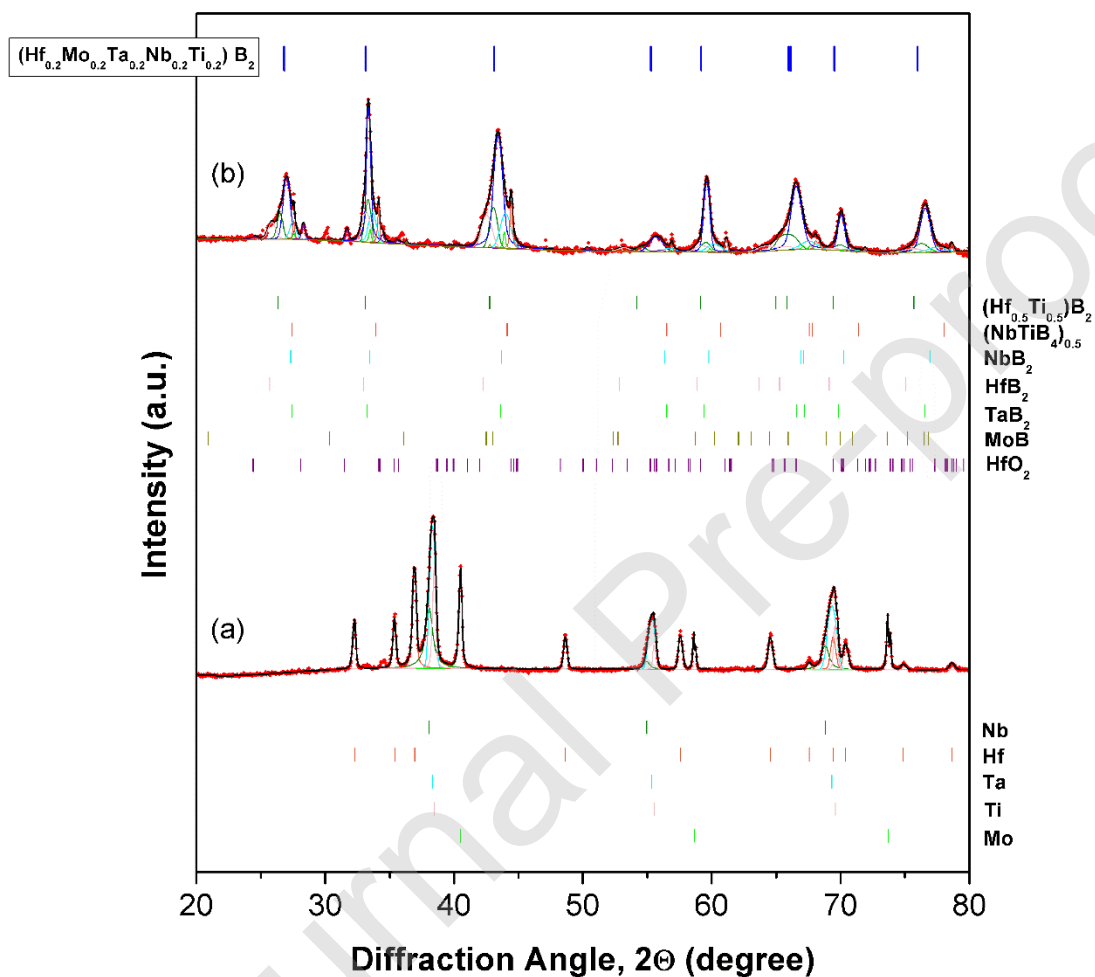


Fig. 3 Temperature and sample displacement (a) time profiles and gas pressure (b) during reactive SPS of $(\text{Hf}_{0.2}\text{Mo}_{0.2}\text{Ta}_{0.2}\text{Nb}_{0.2}\text{Ti}_{0.2})\text{B}_2$ ($T_D = 1950$ A, $P = 20$ to 70 MPa, $HR = 200^\circ\text{C}/\text{min}$, $t_D = 20$ min).

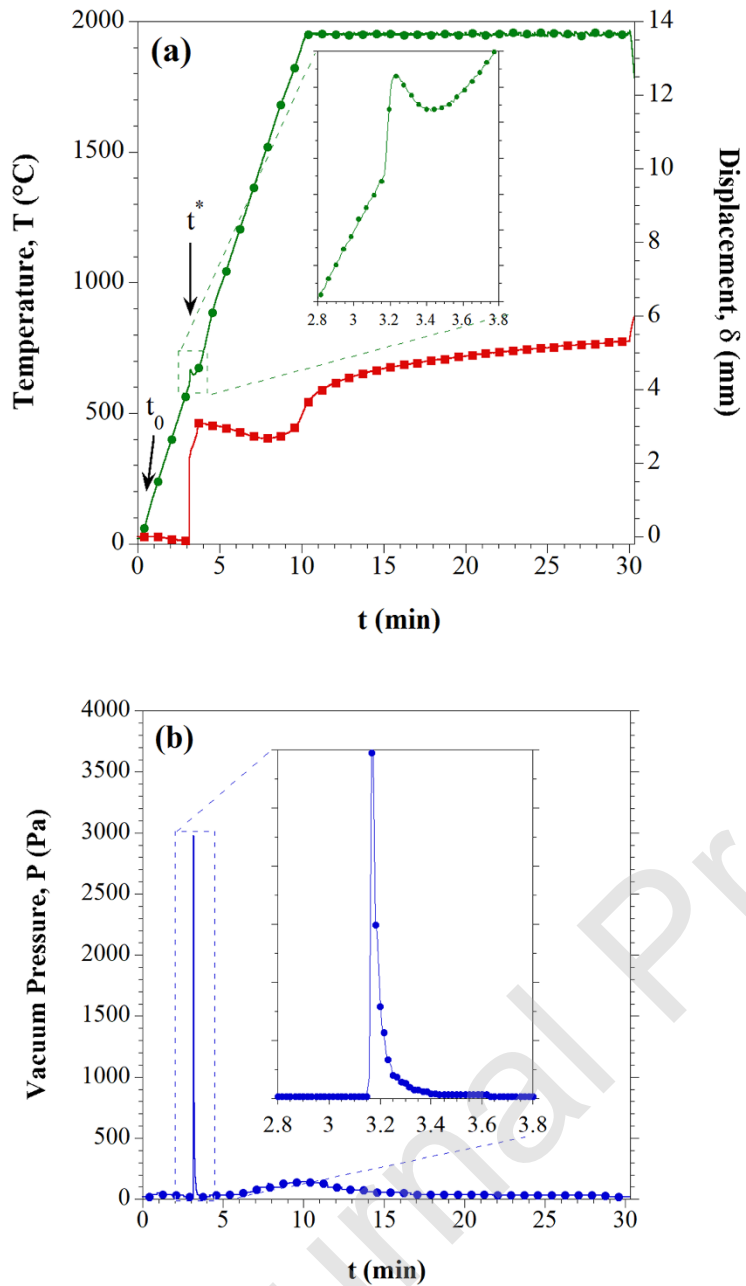


Fig. 4 XRD patterns of (a) reactants and related SPS products ($T_D = 1950\text{A}$, $P = 20\text{MPa}$, $HR = 200^\circ\text{C}/\text{min}$, $t_D = 20$ min) obtained for (b) $x = 0$, (c) $x = 0.1$ and (d) $x = 0.2$ immediately after ($t = t^*$) the sharp sample displacement (**Fig. 3a**) occurring during reactive sintering of $(\text{Hf}_{0.2}\text{Mo}_{0.2}\text{Ta}_{0.2}\text{Nb}_{0.2}\text{Ti}_{0.2})\text{B}_2$.

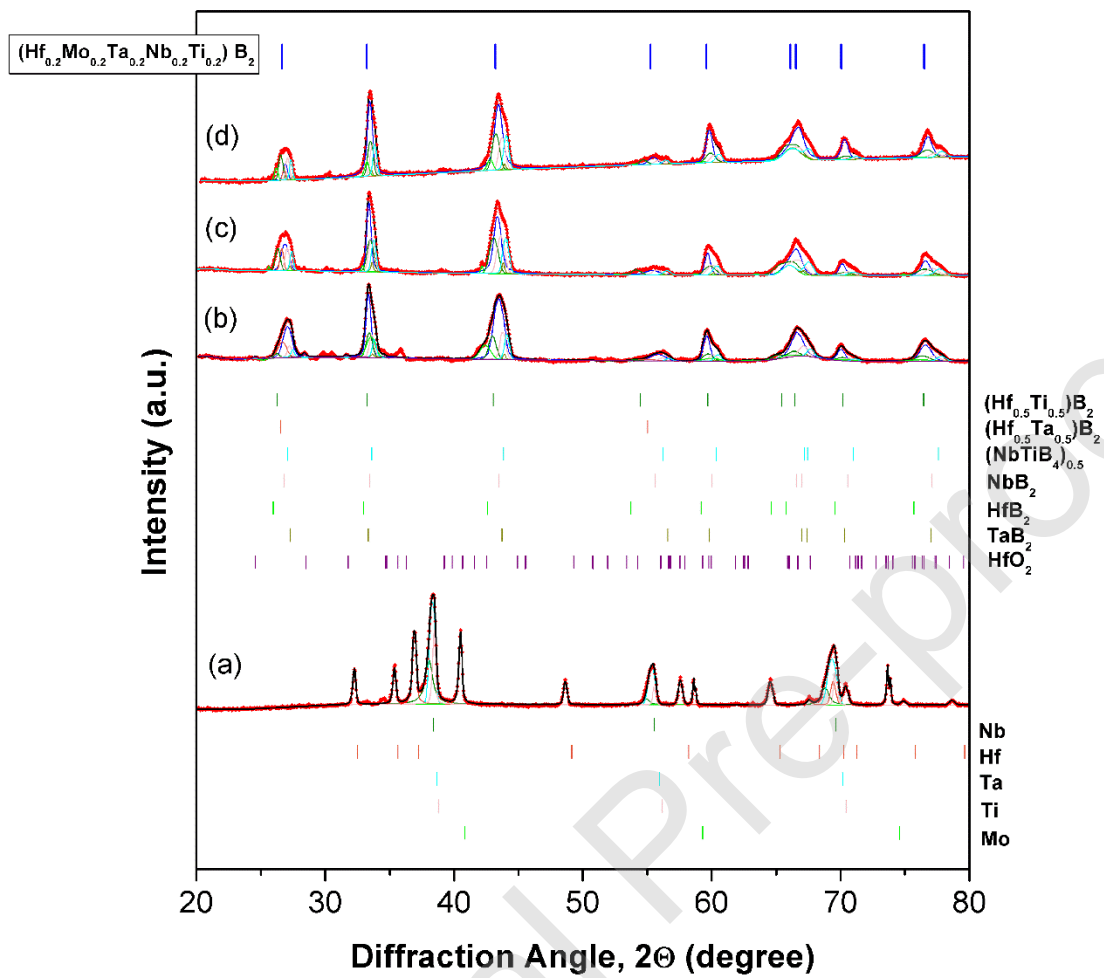


Fig. 5 Densities of sintered products as a function of the mechanical pressure applied after synthesis occurrence during R-SPS ($HR = 200^\circ\text{C}/\text{min}$, $T_D = 1950\text{A}$, $t_D = 20$ min) of $(\text{Hf}_{0.2}\text{Mo}_{0.2}\text{Ta}_{0.2}\text{Nb}_{0.2}\text{Ti}_{0.2})\text{B}_2$.

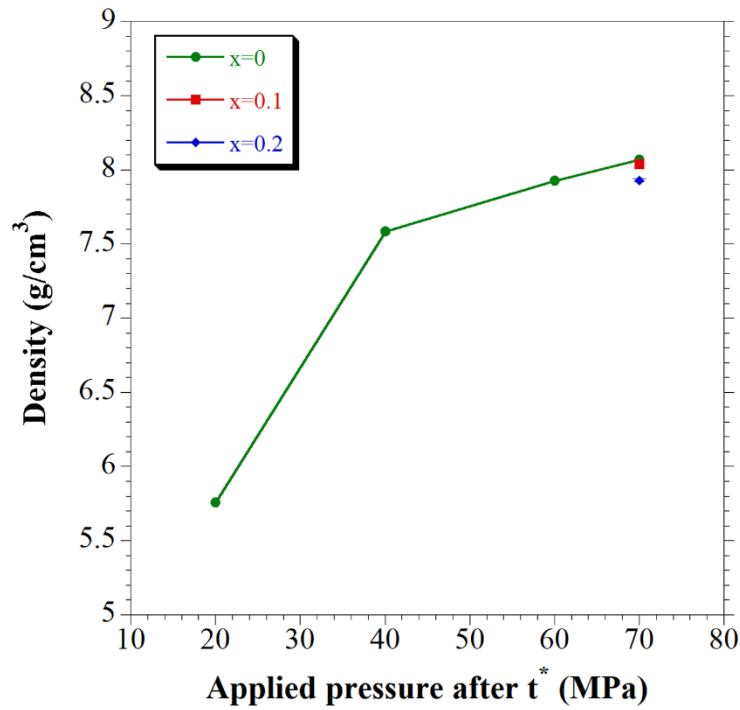


Fig. 6. Cross sectional SEM micrograph and corresponding EDX elemental maps of the $(\text{Hf}_{0.2}\text{Mo}_{0.2}\text{Ta}_{0.2}\text{Nb}_{0.2}\text{Ti}_{0.2})\text{B}_2$ samples produced by R-SPS: (a) ($HR = 100\text{ }^\circ\text{C}/\text{min}$, $T_D = 1950\text{A}$, $t_D = 20$ min, $P = 20$ MPa) and (b) ($HR = 200\text{ }^\circ\text{C}/\text{min}$, $T_D = 1950\text{A}$, $t_D = 20$ min, $P = 20$ to 70 MPa).

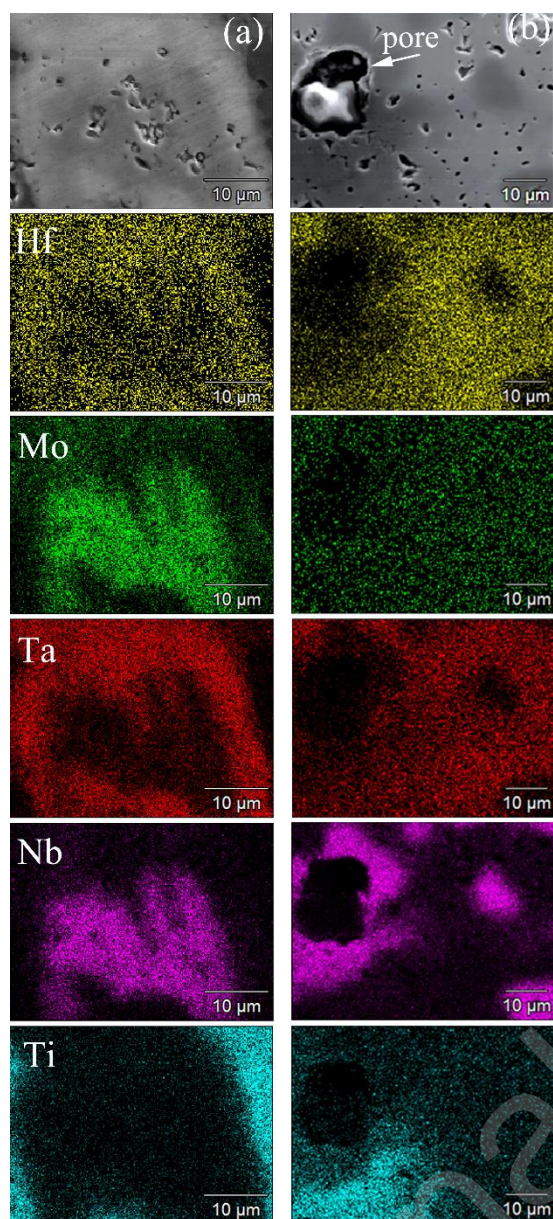


Fig. 7 XRD patterns of products obtained by SHS when (a) $x = 0$, (b) $x = 0.1$ and (c) $x = 0.2$.

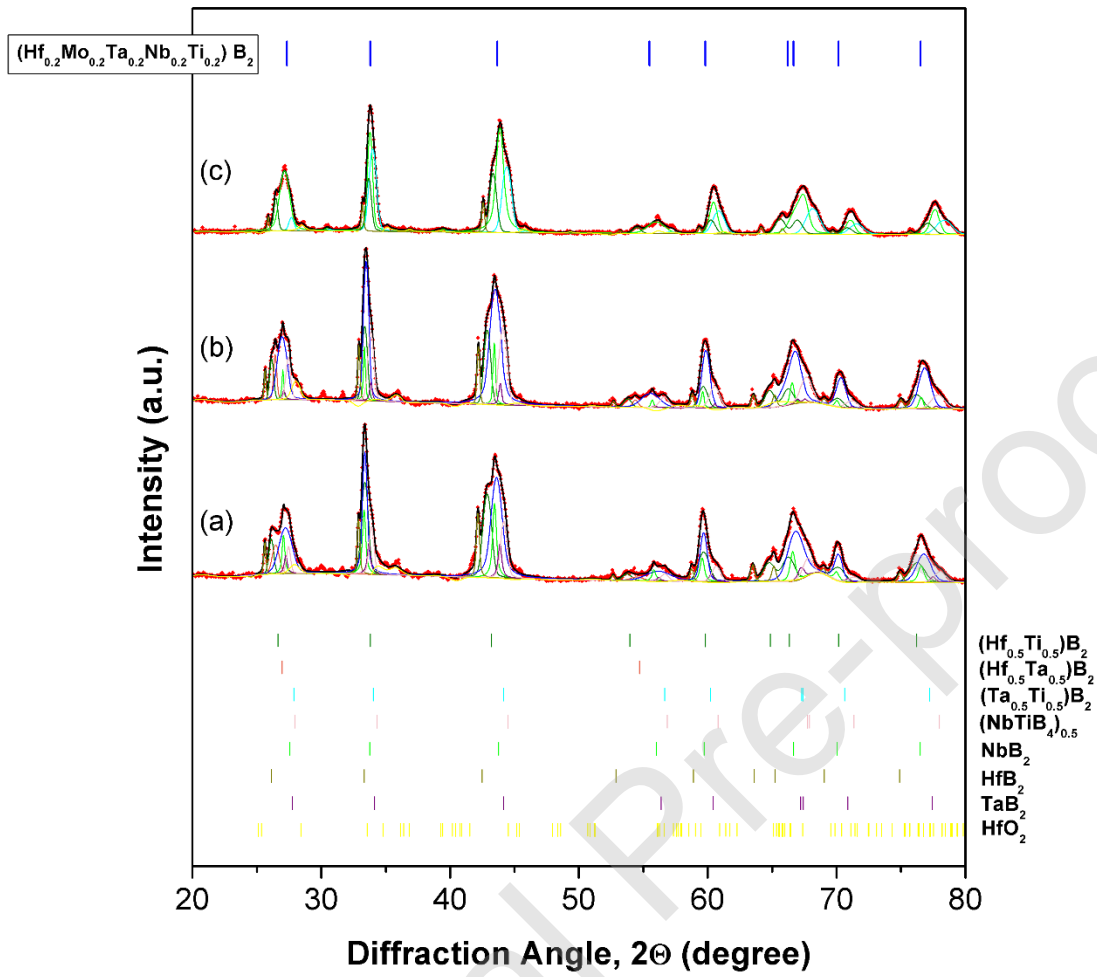


Fig. 8. SEM micrograph and corresponding EDX elemental maps of the SHS powders prepared according to Eq. (1).

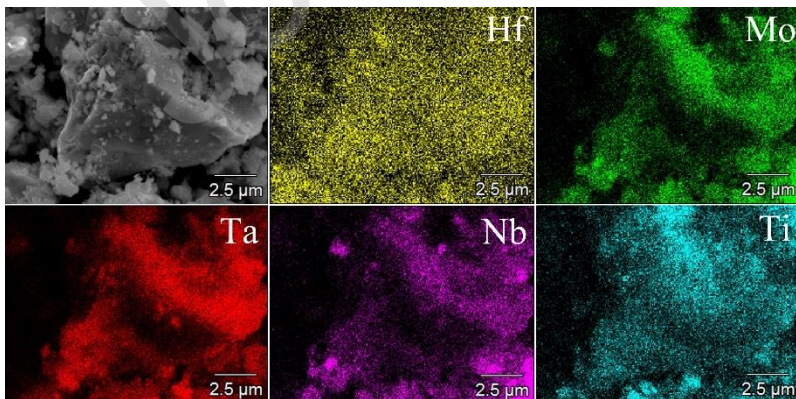


Fig. 9 Example of temperature and sample displacement time profiles during the consolidation by SPS ($T_D = 1950^\circ\text{C}$, $P = 20\text{ MPa}$, $HR = 200^\circ\text{C}/\text{min}$, $t_D = 20\text{ min}$) of SHS powders produced according to Eq. (1).

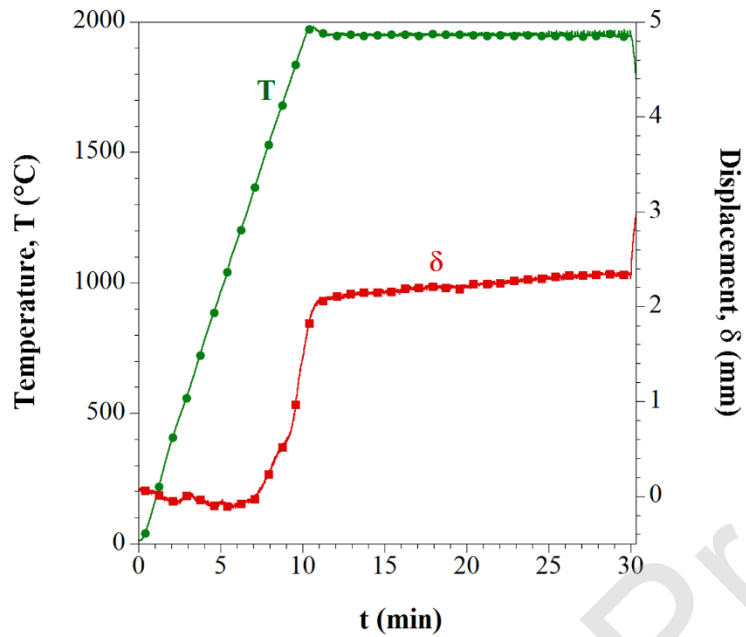


Fig. 10 Effect of the dwell temperature on the density of products obtained by SPS ($P = 20\text{ MPa}$, $HR = 200^\circ\text{C}/\text{min}$, $t_D = 20\text{ min}$) from differently milled SHS powders.

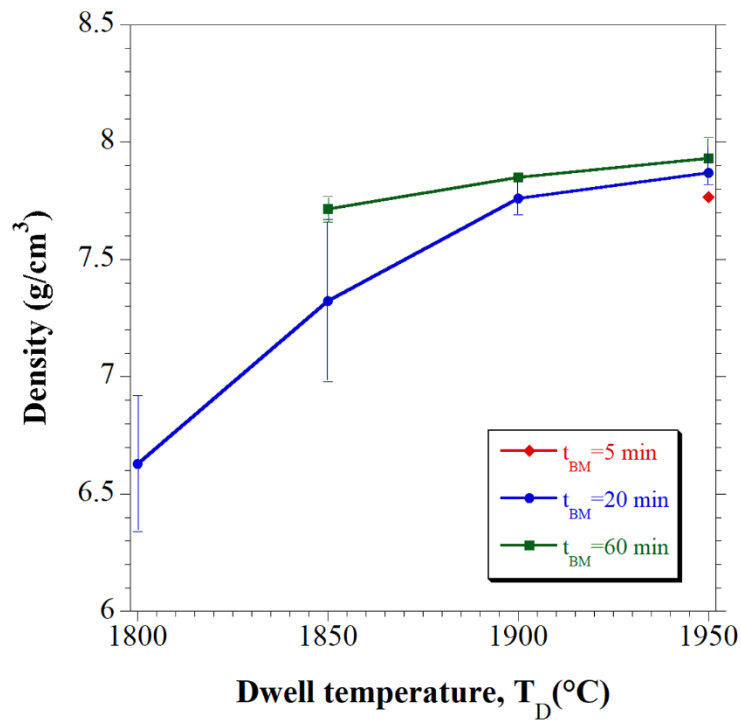


Fig. 11 XRD patterns of (a) the SHS powders ($x = 0.2$, $t_{BM} = 20$ min) and (b) the corresponding SHS-SPS bulk product ($T_D = 1950^\circ\text{C}$, $t_D = 20$ min, $P = 20$ MPa, $HR = 200^\circ\text{C}/\text{min}$).

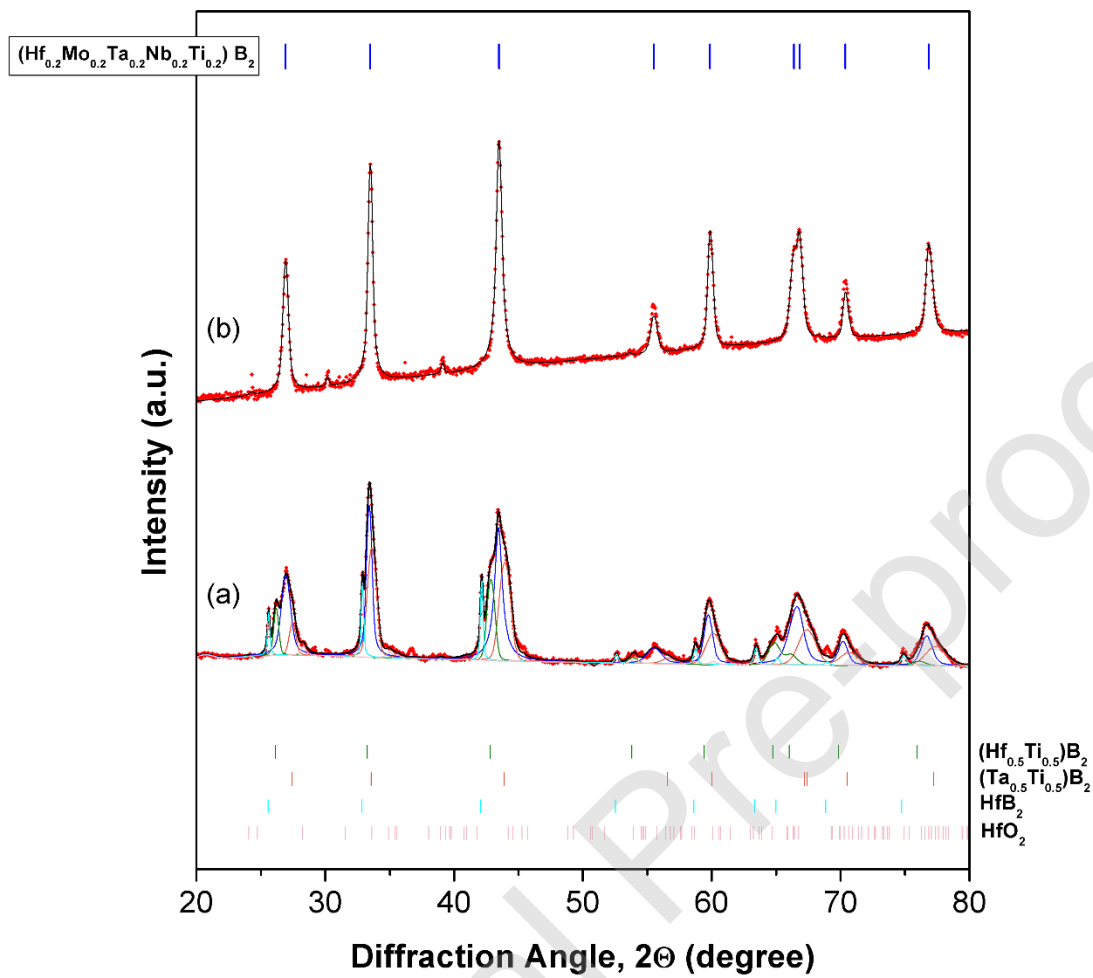


Fig. 12. Cross sectional SEM micrographs and corresponding EDX elemental maps of the $(\text{Hf}_{0.2}\text{Mo}_{0.2}\text{Ta}_{0.2}\text{Nb}_{0.2}\text{Ti}_{0.2})\text{B}_2$ samples produced by SPS ($HR = 200^\circ\text{C}/\text{min}$, $t_D = 20$ min, $P = 20$ MPa) from SHS powders at different conditions: (a) $T_D = 1850^\circ\text{C}$, $t_{BM} = 20$ min; (b) $T_D = 1900^\circ\text{C}$, $t_{BM} = 20$ min; (c) $T_D = 1950^\circ\text{C}$, $t_{BM} = 20$ min; (d) $T_D = 1950^\circ\text{C}$, $t_{BM} = 60$ min.

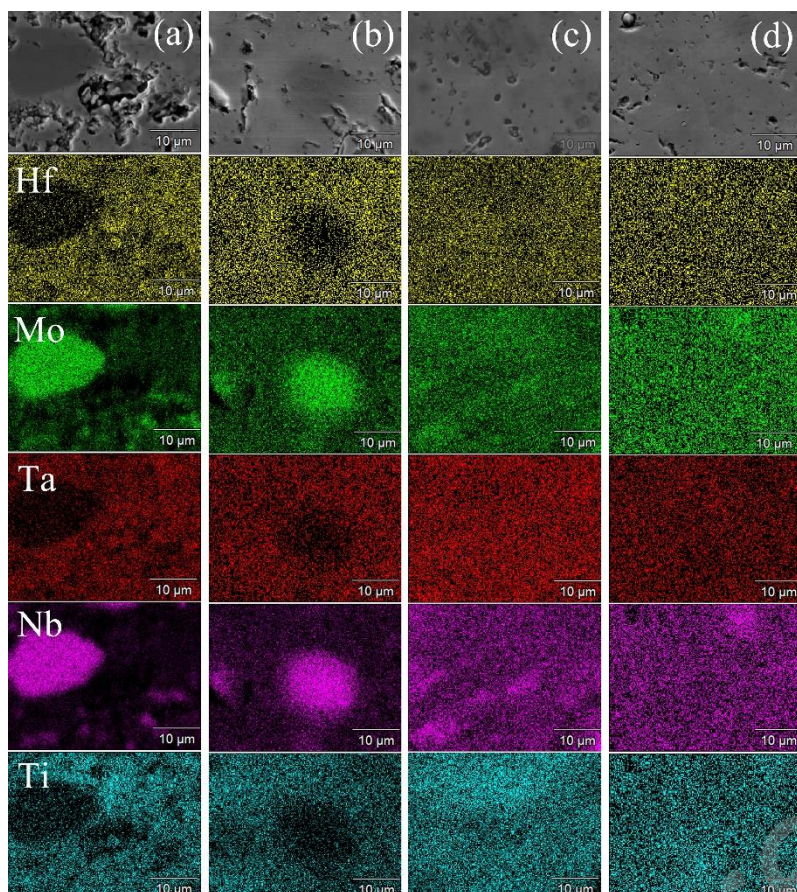


Fig. 13. Comparison of specific weight changes during TGA oxidation in air of $(\text{Hf}_{0.2}\text{Mo}_{0.2}\text{Ta}_{0.2}\text{Nb}_{0.2}\text{Ti}_{0.2})\text{B}_2$ (HEB) and selected individual diborides (HfB_2 , TaB_2 , and TiB_2) as a function of (a) temperature (non-isothermal run with the heating rate equal to $2\text{ }^\circ\text{C}/\text{min}$) and (b) time (isothermal run at $1200\text{ }^\circ\text{C}$).

